The EuroBiotech Journal
RESEARCH ARTICLE
Medical Biotechnology

Transcriptomic Analysis of GLUT10 Deficiency in Arterial Tortuosity Syndrome

Gulden Yorgancioglu Budak[1], Nurdeniz Nalbant[2], Burcu Turkgenc[3], Fahrettin Uysal[4], Ozlem Mehtap Bostan[4], Sebnem Özemri Sag[5], Ergun Cil[4], Sehime G. Temel [2,5*]

Abstract

Arterial Tortuosity Syndrome (ATS) is a rare autosomal recessive connective tissue disorder caused by mutations in the *SLC2A10* gene encoding the glucose transporter GLUT10. GLUT10 deficiency leads to the accumulation of reactive oxygen species (ROS), resulting in oxidative stress, extracellular matrix (ECM) disorganization, and dysregulated signaling that compromise vascular integrity. This study aimed to characterize transcriptomic alterations in fibroblasts derived from ATS patients to elucidate molecular mechanisms underlying the disease and identify potential compensatory responses to ECM disruption. Fibroblasts from two ATS patients carrying homozygous *SLC2A10* missense variants were analyzed by RNA sequencing (RNA-seq). Differential gene expression (DEG) analysis was followed by Kyoto Encyclopedia of Genes and Genomes (KEGG) and Gene Ontology (GO) pathway enrichment analyses to identify altered biological processes. Functional categorization focused on gene sets related to vascular integrity, ECM organization, and cardiovascular function. RNA-seq revealed significant transcriptional dysregulation in ATS fibroblasts compared to controls. Genes involved in Wnt signaling, angiogenesis, and vascular remodeling were significantly upregulated, suggesting potential compensatory mechanisms against ECM disorganization. In contrast, genes related to cardiovascular integrity, ECM-receptor interaction, and basement membrane stability were markedly downregulated. KEGG pathway analysis showed suppression of critical cardiovascular pathways, including hypertrophic cardiomyopathy (HCM), arrhythmogenic right ventricular cardiomyopathy (ARVC), ECM-receptor interaction, and complement and coagulation cascades. Conversely, the upregulation of cell adhesion molecules (CAMs) indicated potential adaptive responses to vascular abnormalities. Our findings demonstrate that *SLC2A10* mutations impair ECM integrity and vascular remodeling, contributing to the molecular pathology of ATS. The observed transcriptional signatures highlight both disrupted pathways and compensatory responses, providing novel insights into ATS pathophysiology and suggesting potential therapeutic targets for future intervention.

Keywords: Arterial Tortuosity Syndrome, *SLC2A10*, GLUT10, RNA-seq, vascular remodeling, gene expression.

[1] Department of Medical Biology, Faculty of Medicine, Istinye University, Istanbul, Turkiye
E-mail: gulden.budak@istinye.edu.tr, ORCID: 0000-0002-3971-2959
[2] Department of Translational Medicine, Bursa Uludag University, Bursa, Turkiye
E-mail: deniznlbnt@gmail.com, ORCID: 0000-0002-9755-6464
[3] Department of Medical Biology, Faculty of Medicine, Uskudar University, Istanbul, Turkiye
E-mail: burcu.turkgenc@uskudar.edu.tr, ORCID: 0000-0001-7306-5866
[4] Department of Pediatric Cardiology, Faculty of Medicine, Bursa Uludag University, Bursa, Turkiye
E-mail: fahrettinuysal@uludag.edu.tr, ombostan@uludag.edu.tr, ergunc@uludag.edu.tr
ORCID: 0000-0002-7747-4859, 0000-0001-7707-2174, 0000-0003-3516-0082
[5] Department of Medical Genetics, Faculty of Medicine, Bursa Uludag University, Bursa, Turkiye
E-mail: ozemri@uludag.edu.tr, sehime@uludag.edu.tr
ORCID: 0000-0002-3948-8889, 0000-0002-9802-0880

***Corresponding author:**
Prof. Sehime G. Temel, MD, PhD
Email: sehime@uludag.edu.tr

DOI: 10.2478/ebtj-2026-0008

© 2026 Authors. This work was licensed under the Creative Commons Attribution-NonCommercial-NoDerivs 3.0 License.

Introduction

Arterial Tortuosity Syndrome (ATS) (MIM#208050), initially identified by Ertugrul in Turkiye nearly 60 years ago, is a rare autosomal recessive connective tissue disorder chiefly characterized by arterial deformities such as tortuosity, elongation, aneurysms, and stenoses that may result in early mortality [1,2]. Other features include skin abnormalities, including softness, hyperextensibility, or cutis laxa, as well as joint laxity, contractures, and distinctive facial features like an elongated face, micrognathia, blepharophimosis, and convex nasal ridge [3,4]. Moreover, corneal thinning and pellucid corneas have been recently described in ATS patients [5,6].

ATS is caused by pathogenic variants in the Solute Carrier Family 2 Member 10 (*SLC2A10*) (MIM#606145) [1,7]. The spectrum of variants in *SLC2A10* includes missense, nonsense, and splice-site mutations, as well as large exonic and small deletions [8,9]. *SLC2A10* encodes the 541-amino acid GLUT10 protein, a class III glucose transporter within the solute carrier 2A (SLC2A) family [1,7,10,11]. High expression levels of GLUT10 mRNA are observed in the liver and pancreas, with significant presence in other essential tissues such as the heart, lungs, brain, skeletal muscle, placenta, and adipose tissue [12,13]. Moreover, GLUT10 is localized to the nuclear envelope [1], endoplasmic reticulum (ER) [14], mitochondria, and Golgi apparatus at the subcellular level [15]. Several disease mechanisms have been suggested. GLUT10 may facilitate the transport of

dehydroascorbic acid (DHA), the oxidized form of the potent antioxidant ascorbic acid (AA), which acts as a cofactor for Lysyl oxidase (like) enzymes and is essential for collagen and elastin cross-linking in the ER [15,16]. Upon being transported into the mitochondrial matrix, DHA is reduced back to AA, which can eliminate reactive oxygen species (ROS), thereby protecting the cell from oxidative stress. Therefore, GLUT10 acts as a cellular defense against oxidative stress by mitigating ROS-induced extracellular matrix (ECM) protein fragmentation [15,17].

GLUT10 deficiency has been associated with enhanced transforming growth factor beta (TGF-β) pathway activity in the arterial wall characterized by its association with aortic aneurysms and arterial tortuosity [18]. Moreover, the decreased expression of decorin in cultured vascular smooth muscle cells (SMCs) from ATS patients results in an elevation of TGF-β-driven expression of versican, a proteoglycan that inhibits elastic fiber assembly [1,19], which may contribute to impaired elastogenesis in ATS.

Skin biopsies from ATS patients show that the elastin core of elastic fibers was disorganized and infiltrated by microfibrils [7]. Additionally, cultured fibroblasts showed disorganization in the actin cytoskeleton and changes in various ECM components, including fibronectin, fibrillin, type III collagen, type V collagen, and decorin [1,7,20,21].

In zebrafish embryos, the inhibition of *slc2a10* through antisense morpholino oligonucleotide injection resulted in a notochord exhibiting waviness alongside cardiovascular anomalies characterized by decreased heart rate and blood flow, concomitant with incomplete and irregular vascular patterning [22]. Mice homozygous for missense substitutions in *GLUT10* do not exhibit the severe vascular abnormalities observed in human ATS patients, thus limiting their utility in exploring the pathogenetic mechanisms of human ATS [23]. To overcome species-specific differences in ascorbic acid metabolism, a double knock-out mouse model was generated for targeting both *Slc2a10* and *Gulo*, the latter being essential for endogenous ascorbic acid biosynthesis in mice. Although this model did not fully recapitulate the vascular manifestations of human ATS, it revealed subtle histological abnormalities, impaired extracellular matrix deposition, and reduced mitochondrial respiration in vascular smooth muscle cells [24].

In the present study, we aimed to investigate transcriptomic alterations in skin fibroblasts derived from two patients with ATS carrying homozygous missense variants in *SLC2A10*, along with their carrier parents. To explore the molecular pathways potentially involved in ATS pathophysiology, gene expression profiling and pathway enrichment analyses were performed using fibroblasts obtained from Patient 1 and Patient 2.

2. Materials and methods

2.1. Ethical Approval

This study was approved by the Bursa Uludag University Health Research Ethics Committee (Decision Number: 2026/189/6-36). Written informed consent was obtained from the legal guardians of the patients and from carrier parents for the publication of photographs and the collection, storage, analysis, and use of biological materials and associated data.

2.2. Clinical Assessment

Two patients diagnosed with ATS were clinically evaluated. Clinical information, conventional angiography images, and Magnetic Resonance Angiography (MRA) data were retrospectively obtained.

2.3. DNA Extraction

Genomic DNA was isolated from peripheral venous blood samples obtained from Patient 1, Patient 2, the parents of Patient 1, and the mother of Patient 2. In the case of Patient 2, the DNA was obtained solely from the mother. The extraction was performed using the QIAamp® DNA Mini Kit (QIAGEN, Ankara, Turkey), following the manufacturer's standard protocol.

2.4. Whole Exome Sequencing (WES)

SureSelectXT Library Prep Kit (Agilent Technologies, San-ta Clara, CA, USA) was utilized for target enrichment of the protein-coding regions of the genome for WES. All procedures were carried out according to the manufacturer's protocols. Paired-end sequencing was performed on an Illumina NovaSeq platform (Illumina, San Diego, CA, USA) with a read length of 151 base pairs. Base calling and image analysis were conducted using Illumina's Real-Time Analysis software. The binary base call (BCL) generated by the sequencing instru-ment was then converted into FASTQ format, which contains the sequence data and corresponding quality scores, utilizing Illumina's bcl2fastq package. Moreover, *SLC2A10* mutations, along with variant confirmation and segregation analyses, were performed by Sanger sequencing on a genetic analyzer (Thermo Fisher Scientific, Waltham, MA, USA) according to the manufacturer's protocol. Variant interpretation was performed according to the American College of Medical Genetics and Genomics (ACMG) guidelines [25].

2.5.Bioinformatics Analyses

All bioinformatics analyses were performed on the SOPHiA DDM™ platform (SOPHiA Genetics, Lausanne, Switzerland), which includes algorithms for alignment, calling single nucleotide polymorphisms (SNPs) and small indels (Pepper), calling copy number variations (Muskat), and functional annotation (Moka). Raw reads were aligned to the human reference genome (GRCh37/hg19). Variant filtering and interpretation were performed on SOPHiA DDM™ platform.

2.6. Cultured fibroblasts

A 4-mm punch skin biopsy was taken under local anesthesia from the patients [26]. All tissue processing steps were

performed under sterile conditions in a laminar flow hood. The skin biopsies were dissected into approximately 12–15 evenly sized (~0.5 mm) pieces using sterile scalpel blades, ensuring smooth edges to promote optimal tissue attachment and cell outgrowth, as previously described [27] . These tissues were incubated at 37°C in a humidified incubator with 5% CO2, in a minimal volume of growth media composed of Dulbecco's Modified Eagle Medium (DMEM; Gibco, Thermo Fisher Scientific, W altham, MA, USA), 10% fetal bovine serum (FBS; Gibco, Thermo Fisher Scientific, Wa ltham, MA, USA), 1 mM sodium pyruvate (Gibco, Thermo Fisher Scientific, Waltham, MA, USA), 4 mM L-glutamine (Gibco, Thermo Fisher Scientific, Wa ltham, MA, USA), pe nicillin–streptomycin (Gibco, Thermo Fisher Scientific, Wa ltham, MA, USA), and 2.5 µg/ml amphotericin B (Sigma-Aldrich, St. Louis, MO, USA). During the first week, medium volume was carefully maintained to ensure adequate surface coverage, with gradual addition of fresh medium. After initial attachment and outgrowth, the medium volume was increased to 2 ml and replaced every 2–3 days. Fibroblast outgrowth was monitored, and cells were cultured for approximately four weeks until sufficient confluency was achieved for further passaging [27] .

2.7. RNA Extraction and RNA-Seq Library Preparation

Total RNA was extracted from fibroblasts samples using the NucleoSpin RNA Purification Kit (Macherey-Nagel, Germany) following the manufacturer's instructions. To enrich the poly(A)-tailed RNA population, 2.0 µg of total RNA from each sample was processed using the Poly(A) mRNA Magnetic Isolation Module kit (New England Biolabs, USA) [28]. Paired-end sequencing (100 bp) of cDNA libraries from the fibroblast samples was performed in two biological replicates using the Illumina HiSeq2500 platform (Illumina, San Diego, CA, USA) through a commercial sequencing service (Macrogen Europe B.V., Netherlands).

2.8. RNA-Seq Analysis

RNA-seq analysis was performed following the protocols [29-31]. Raw sequencing reads were assessed using the FastQC software (Babraham Bioinformatics, UK). Trimmomatic (v0.35) was employed to remove low-quality bases (quality score < Q30) and any adaptor contamination [30]. The resulting high-quality sequence data, consisting of 2 × 100 bp paired-end reads, were saved in FASTQ format (Supp. Fig. 1). Then, the reads were aligned to the human reference genome GRCh38 using the STAR aligner (v2.5.2; Cold Spring Harbor Laboratory, NY, USA) [32]. Transcript-level R^2 values between replicates for each condition were determined through correlation analysis using the heatmap.2 function in R. Differentially expressed genes (DEGs) across conditions were identified using the Cuffdiff command from the Cufflinks suite [33], applying default parameters and a false discovery rate (FDR) threshold of ≤ 0.01. The differential expression analysis was performed using quartile library normalization and pooled dispersion estimation methods, and fragments per kilobase of transcript per million mapped reads (FPKM) and fold changes were calculated. DEGs exhibiting |log2 fold change| > 0.5 were further analyzed to identify significant differences between fibroblast samples.

2.9. KEGG pathway enrichment analysis

The ClueGO extension of Cytoscape (v3.6.0; Institute for Systems Biology, Seattle, WA, USA) was employed to identify significantly altered KEGG pathways from each list of differentially expressed genes (DEGs), with a significance threshold set at a p-value of ≤ 0.05 [28,30,34].

3. Results

3.1. Patient History

3.1.1. Family 1

Patient 1 presented with loose skin, joint laxity, scoliosis, delayed wound healing, hernias, and notable facial features such as a long face, convex nasal ridge, microretrognathia, sagging cheeks, a long philtrum, a highly arched palate, hypertelorism, broad ears, and malar hypoplasia (Figure 1A,B). He also presented with joint hyperlaxity and dolichostenomelia of the lower extremities.

An aneurysmal enlargement of the ascending aorta was observed in Patient 1, accompanied by hypoplasia in the descending aorta and aortic arch. Elongation and tortuosity were observed in the bilateral internal carotid arteries and their branches, with similar findings in the posterior fossa arteries, and the basilar artery was diffusely thin Figure (1C+). MRA revealed a collateral connection between the hepatic vein and the inferior vena cava in Patient 1 (Figure 2A). MRI revealed a sequela infarct area located in the left lentiform nucleus-corona radiata region, along with mild dilation of the left lateral ventricle (Figure 2B). Furthermore, ocular examination showed keratoconus, corneal clouding, Descemet's membrane striae, and superior scleromalacia (data not shown).

3.1.2. Family 2

Patient 2 presented with mild scoliosis, pectus deformity, microretrognathia, sagging cheeks, malar hypoplasia and a beaked nose (Figure 3A). Conventional angiography revealed elongated, tortuous segments of the aorta (Figure 3B). Ophthalmological examination showed increased bilateral retinal arterial tortuosity (data not shown).

3.2. Molecular Analysis

Whole exome sequencing identified a homozygous missense variant c.727C>A (p.Gln243Lys) in the *SLC2A10* gene (NM_030777.4) in Patient 1 (Figure 4A), and a homozygous missense variant c.395G>A (p.Arg132Gln) in the *SLC2A10* gene (NM_030777.4) in Patient 2 (Figure 4B). The *SLC2A10* variant c.727C>A was classified as likely pathogenic (LP) according to ACMG criteria, supported by PM2 (absent or extremely rare in population databases), PM3 (for recessive disorders, detected in trans with a pathogenic variant), and PP3 (multiple lines of computational evidence support a deleterious

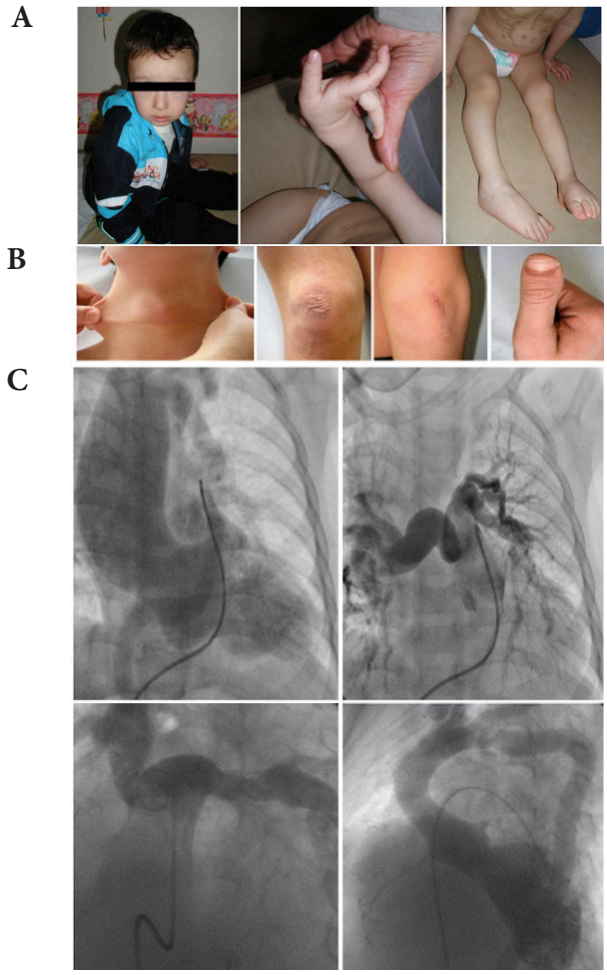


Figure 1. Clinical anomalies in Patient 1. A) Facial and skeletal features include sagging cheeks, malar hypoplasia, micrognathia, joint hyperlaxity, and elongated lower extremities. B) Loose skin, joint laxity and delayed wound healing. C) Conventional angiography of Patient 1 demonstrates an aneurysmatic widening of the ascending aorta and aortic arch, accompanied by a thin and tortuous descending aorta.

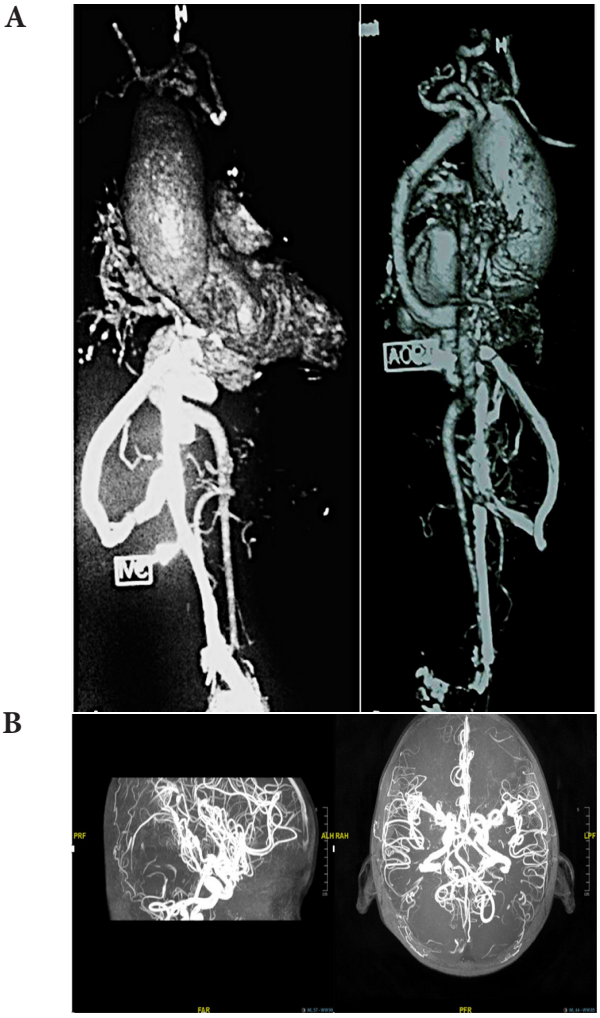


Figure 2. Radiological findings in Patient 1. A) Magnetic resonance angiography (MRA) images of Patient 1 showing a collateral connection between the hepatic vein and the inferior vena cava. B) Cranial magnetic resonance imaging (MRI).

effect on the gene or gene product) [27]. Also, the *SLC2A10* variant c.395G>A was classified as LP according to ACMG criteria, supported by PM2, PM5 (novel missense change at an amino acid residue where a different missense change determined to be pathogenic has been seen before), PP3, and PM1 (located in a mutational hot spot and/or critical and well-established functional domain without benign variation) [27]. Segregation analysis revealed that both parents of Patient 1 and the mother of Patient 2 were heterozygous carriers.

3.3. Comparative RNA-seq Expression Profiles in ATS Patients

We performed RNA-seq analysis using fibroblasts derived from skin biopsies obtained from Patient 1, Patient 2, and both parents of Patient 1, and the mother of Patient 2. The hierarchical clustering on the left side of Figure 5A/B represents the grouping of genes based on similarities in their expression profiles across the samples. Genes with similar expression patterns across patients and controls are clustered together, facil-

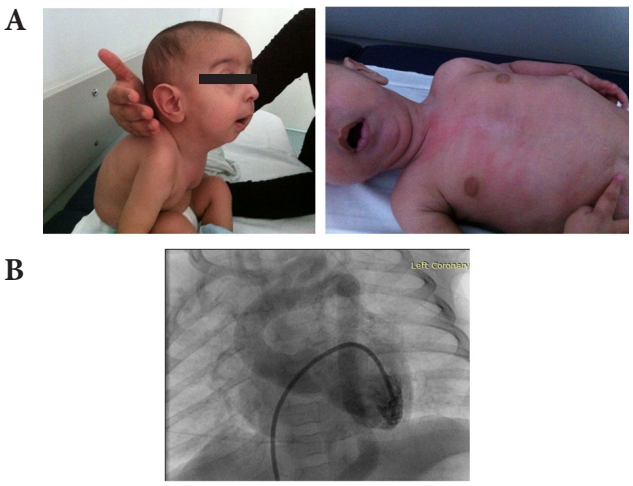


Figure 3. Clinical anomalies in Patient 2. A) Pectus deformity, micro-retrognathia, sagging cheeks, malar hypoplasia, and a convex nasal ridge. B) Conventional angiography revealing elongated, tortuous segments of the aorta.

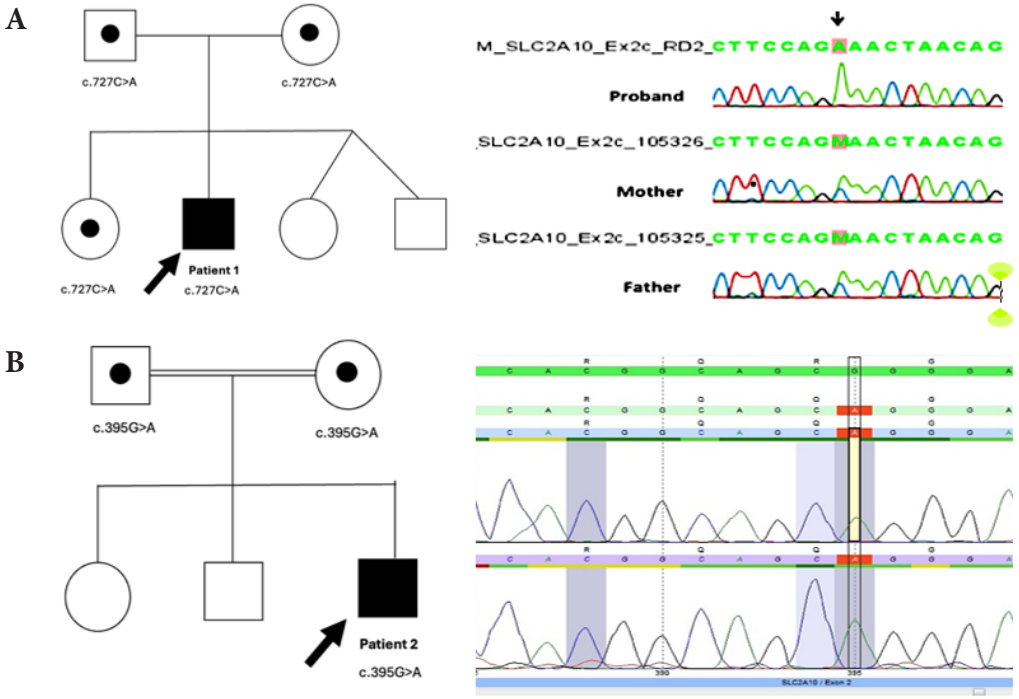


Figure 4. Pedigrees and Sanger sequencing results of families with ATS Patients. A) Pedigree chart and Sanger sequencing results of Family 1, showing segregation of the homozygous c.727C>A variant in Patient 1, validated by Sanger sequencing of *SLC2A10* Exon 2. B) Pedigree chart of Family 2, illustrating segregation of the homozygous c.395G>A variant in Patient 2, with Sanger sequencing results showing heterozygosity in the mother.

itating the identification of co-regulated or functionally related genes. Patient 1 was compared with the patient's mother and father, while Patient 2 was compared with the patient's mother, as outlined in Table 1. The heat map illustrates the comparative expression profiles of Patient 1 and the carrier parents, highlighting specific genes that are both up-regulated and down-regulated (Figure 5A).

A comparable expression profile was observed for Patient 2 and the patient's mother, with distinct clusters of differentially expressed genes separating the patient, as visualized by the hierarchical clustering (Figure 5B). Moreover, common up-regulated and down-regulated genes were found in both patients (Figure 5C). The Venn diagram illustrates the overlap and unique RNA-seq results obtained from the two patients. Bioinformatic analyses identified 700 DEGs unique to Patient 1 and 944 unique to Patient 2, with 230 DEGs common to both, highlighting the specific and overlapping molecular pathways in GLUT10 deficiency (Figure 5D).

RNA-seq analysis of fibroblast samples from Patients 1 and 2 led to the identification of several genes with significant fold changes in their expression levels (Table 1). Several genes such as *SFRP1*, *GPR37*, and *STMN3* were found to be highly up-regulated, indicating a notable increase in their expression. Conversely, *ADH1B*, *TNNT2*, and *COL4A4* genes were significantly down-regulated, demonstrating substantial decreases in their expression levels.

3.4. KEGG and Gene Ontology Pathway Analysis

To identify the biological processes, we evaluated significantly altered KEGG pathways. In our analysis, significant down-regulation was observed in crucial immune and inflammatory pathways in Patient 1 (Table 2). Key pathways such as TNF signaling and NF-kappa B, which are essential for inflammatory responses, along with the NOD-like receptor signaling pathway and complement and coagulation cascades, were notably downregulated. Conversely, the CAMs pathway was down-regulated in Patient 1 but was up-regulated in Patient 2, suggesting variable changes in cellular adhesion properties (Table 2).
Notably, there was a significant down-regulation in pathways linked to cardiovascular diseases, such as HCM and ARVC, highlighting potential cardiac vulnerabilities in Patient 2 (Table 2). Additionally, other crucial pathways including ECM-receptor interaction and complement and coagulation cascades were also down-regulated, impacting cellular interactions and immune responses.

Gene Ontology (GO) Pathways analysis for Biological Processes (BP) in Patient 1 identified down-regulation of pathways crucial for immune and structural integrity in Patient 1 (Table 3). These included the positive regulation of epithelial cell proliferation, angiogenesis, cellular response to retinoic acid, and ECM organization, along with processes such as collagen catabolic process, positive regulation of protein kinase B signaling, and inflammatory response. Additionally, critical immune signaling pathways such as type I interferon signaling,

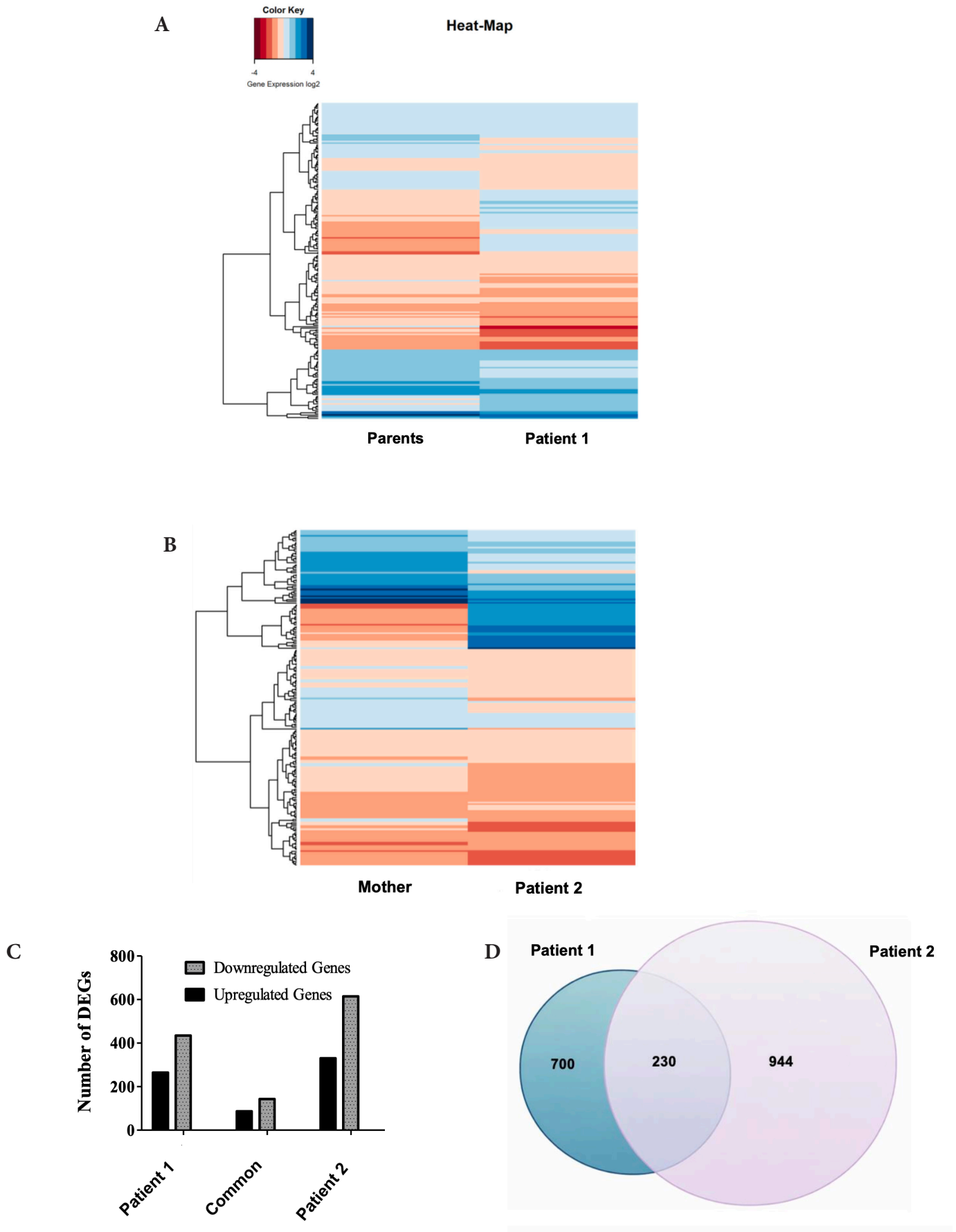


Figure 5. Comparison of RNA Sequencing Analysis of ATS families. A) Heat map of the comparative expression profiles of Patient 1 and his parents. B) Heat map of the comparative expression profiles of Patient 2 and the mother. In both panels, rows represent genes and columns represent individual samples. Hierarchical clustering was performed based on similarity in gene expression patterns. Blue indicates lower expression and red indicates higher expression. C) Bar plot showing the number of differentially expressed genes (DEGs) in Patient 1 and Patient 2. D) Venn diagram showing the overlap of DEGs between Patient 1 and Patient 2, with 230 commonly dysregulated genes.

Table 1. Comparative analysis of the top up-regulated and down-regulated genes in fibroblast samples of Patient 1 and Patient 2.

Up-Regulated Genes	Fold Change	Down-Regulated Genes	Fold Change
SFRP1	7.31	*ADH1B*	-7.71582
GPR37	5.92	*TNNT2*	-5.44062
STMN3	4.23	*COL4A4*	-5.40003
PTPRN	3.99	*AKR1C3*	-5.08512
NTRK2	3.94	*TNFSF15*	-5.05803
SSX2IP	3.83	*SFTA1P*	-5.03233
EPHB2	3.79	*CXCL8*	-5.00475
EFNB2	3.77	*DIO3OS*	-4.68145
MAB21L1	3.65	*C3*	-4.65439
GAP43	3.65	*KRT18*	-4.64753
TNFSF4	3.27	*KRT14*	-4.4855
PITPNM3	2.93	*CCL2*	-4.4165
PHKA1	2.92	*GDF10*	-4.28965
FLT1	2.88	*SBSPON*	-4.28266
GIPC3	2.86	*CXCL1*	-4.24959
CES1	2.82	*TMEM176B*	-4.22315
TMTC2	2.81	*PDE1A*	-4.21258
PITX2	2.81	*OAS1*	-4.17414
DKK1	2.69	*IL20RA*	-4.17245
FBN2	2.65	*FMO3*	-4.09248
FOXE1	2.52	*HGF*	-4.064
AP1S2	2.51	*CLDN1*	-3.98715
TOX2	2.41	*BST2*	-3.98427

Table 2. Changes in up-regulated and down-regulated KEGG pathways in Patient 1 and Patient 2 fibroblasts with False Discovery Rate (FDR) < 0.05.

KEGG pathway name	DEGs Count	P-value	Level
Patient 1			
TNF signaling pathway	14	1.06E-08	DR
Herpes simplex infection	16	1.83E-07	DR
Influenza A	15	6.12E-07	DR
NF-kappa B signaling pathway	11	1.08E-06	DR
Cell adhesion molecules (CAMs)	13	2.46E-06	DR
NOD-like receptor signaling pathway	8	2.45E-05	DR
Complement and coagulation cascades	10	8.98E-06	DR
Patient 2			
Hypertrophic cardiomyopathy (HCM)	15	2.30E-06	DR
ECM-receptor interaction	15	8.76E-06	DR
Complement and coagulation cascades	13	1.72E-05	DR
Arrhythmogenic right ventricular cardiomyopathy (ARVC)	13	2.33E-05	DR
Cell adhesion molecules (CAMs)	13	8.0E-05	UR

DEGs: Differentially Expressed Genes, DR: Down-regulated, UR: Up-regulated

defense response to virus, interferon-gamma-mediated signaling, immune response, and negative regulation of viral genome replication were also down-regulated. Conversely, pathways associated with cell cycle progression and cellular structure, such as mitotic nuclear division, G1/S transition of mitotic cell cycle, and cell adhesion, were found to be upregulated.

In Patient 2, down-regulated pathways include critical processes such as ECM organization, cell adhesion, angiogenesis, collagen fibril organization, signal transduction, negative regulation of cell proliferation, platelet degranulation, skeletal system development, and single organismal cell-cell adhesion (Table 3). These findings suggest a reduction in key cellular activities that are essential for maintaining structural integrity and proper cellular functioning.

Table 3. Up-regulated and Down-regulated GO Annotation pathways based on biological processes (BP) in Patient 1 and Patient 2 fibroblasts with False Discovery Rate (FDR) < 0.05.

GO pathway Based on BP	DEGs Count	P-value	Level
Patient 1			
Positive regulation of epithelial cell proliferation	10	1.29E-06	DR
Angiogenesis	17	3.47E-06	DR
Cellular response to retinoic acid	10	4.83E-06	DR
Extracellular matrix organization	15	1.50E-05	DR
Collagen catabolic process	9	2.03E-05	DR
Positive regulation of protein kinase B signaling	10	2.19E-05	DR
Inflammatory response	21	2.21E-05	DR
Type I interferon signaling pathway	25	2.99E-28	DR
Defense response to virus	22	2.75E-14	DR
Response to virus	18	3.34E-13	DR
Interferon-gamma-mediated signaling pathway	14	2.32E-11	DR
Immune response	26	2.23E-09	DR
Negative regulation of viral genome replication	10	4.28E-09	DR
Mitotic nuclear division	14	4.30E-06	UR
G1/S transition of mitotic cell cycle	9	1.83E-05	UR
Cell adhesion	15	1.83E-05	UR
Patient 2			
Extracellular matrix organization	36	1.40E-14	DR
Cell adhesion	45	1.50E-08	DR
Response to hypoxia	25	3.33E-08	DR
Angiogenesis	28	9.70E-08	DR
Positive regulation of angiogenesis	19	3.04E-07	DR
Inflammatory response	36	1.10E-06	DR
Collagen fibril organization	11	1.31E-06	DR
Signal transduction	77	1.73E-06	DR
Negative regulation of cell proliferation	36	2.98E-06	DR
Response to drug	30	4.88E-06	DR
Platelet degranulation	16	7.33E-06	DR
Skeletal system development	18	1.65E-05	DR
Single organismal cell-cell adhesion	15	2.61E-05	DR
Angiogenesis	22	1.43E-08	UR
Positive regulation of cell proliferation	30	2.84E-07	UR
Positive regulation of cell migration	18	4.56E-07	UR
Cell adhesion	29	6.81E-07	UR
Collagen catabolic process	11	9.56E-07	UR
Extracellular matrix organization	17	5.06E-07	UR
Negative regulation of epithelial cell proliferation	9	2.34E-05	UR

DEGs: Differentially Expressed Genes, DR: Down-regulated, UR: Up-regulated

Conversely, up-regulated pathways were identified in processes including the positive regulation of cell proliferation, cell migration, cell adhesion, the collagen catabolic process, ECM organization, and the negative regulation of epithelial cell proliferation.

In the GO annotation pathway analysis based on Cellular Components (CC) and Molecular Functions (MF), the extracellular space, extracellular region, and extracellular matrix (ECM) were downregulated in both Patient 1 and Patient 2, whereas the cell periphery was upregulated only in Patient 1 (Table 4). However, proteinaceous extracellular matrix was found both up-regulated and down regulated according to CC analysis (Table 4). In Patient 2, pathways related to extracellular interactions and structures were differentially regulated.

Pathways associated with the extracellular space, extracellular region, cell surface, and extracellular exosome were notably downregulated, whereas focal adhesion and extracellular region showed upregulation. Intriguingly, components such as the extracellular matrix, proteinaceous extracellular matrix, plasma membrane, and the integral component of the plasma membrane showed both up-regulation and down-regulation, indicating complex regulatory dynamics in these cellular areas. Furthermore, our MF analysis revealed down-regulation in critical functions such as heparin binding, double-stranded RNA and 2'-5'-oligoadenylate synthetase activity in Patient 1 (Table 5).

Table 4. Up-regulated and down-regulated GO annotation pathways based on cellular components (CC) in Patient 1 and Patient 2 fibroblasts with False Discovery Rate (FDR) < 0.05.

GO pathway Based on CC	DEGs Count	P-value	Level
Patient 1			
Extracellular space	70	4.06E-16	DR
Extracellular region	76	2.64E-15	DR
Proteinaceous extracellular matrix	24	4.31E-10	DR
Extracellular matrix	22	7.11E-08	DR
Cell periphery	7	4.02E-06	UR
Proteinaceous extracellular matrix	13	2.62E-06	UR
Patient 2			
Extracellular space	7	3.81E-19	DR
Proteinaceous extracellular matrix	41	2.11E-14	DR
Extracellular region	112	1.57E-11	DR
Plasma membrane	222	3.70E-11	DR
Cell surface	45	4.86E-07	DR
Extracellular matrix	30	1.17E-06	DR
Extracellular exosome	146	3.14E-06	DR
Integral component of plasma membrane	83	1.27E-05	DR
Receptor complex	17	1.37E-05	DR
Extracellular matrix	27	5.44E-10	UR
Proteinaceous extracellular matrix	22	1.82E-07	UR
Focal adhesion	26	6.04E-07	UR
Integral component of plasma membrane	54	1.53E-05	UR
Plasma membrane	121	1.53E-05	UR
Extracellular region	58	3.59E-05	UR

DEGs: Differentially Expressed Genes, DR: Down-regulated, UR: Up-regulated

Table 5. Up-regulated and down-regulated GO annotation pathways based on Molecular Functions (MF) in Patient 1 fibroblasts with False Discovery Rate (FDR) < 0.05.

GO pathway Based on MF	DEGs Count	P-value	Level
Patient 1			
Heparin binding	17	2.46E-08	DR
Double-stranded RNA binding	9	1.95E-06	DR
2'-5'-oligoadenylate synthetase activity	4	1.05E-05	DR
Patient 2			
Heparin binding	25	6.10E-09	DR
Extracellular matrix structural constituent	15	1.38E-07	DR
Calmodulin binding	23	2.32E-06	DR
Growth factor activity	20	1.01E-05	DR
Collagen binding	12	1.16E-05	DR
Heparin binding	15	7.15E-06	UR

DEGs: Differentially Expressed Genes, DR: Down-regulated, UR: Up-regulated

Also, ECM structural constituent, calmodulin binding, growth factor activity, and collagen binding were downregulated in Patient 2 (Table 5).

Heparin binding, which is crucial for interaction with blood components, was found to be both upregulated and downregulated, reflecting varied influences on this molecular function across different conditions.

4. Discussion

ATS is characterized by arterial deformities such as tortuosity and aneurysms, skin softness, joint laxity, distinctive facial features, and corneal thinning [1,6]. Despite the established genetic link of ATS to mutations in *SLC2A10*, which encodes the GLUT10 transporter, the mechanisms driving connective tissue disorganization in this condition remain poorly defined. To further explore the molecular consequences of *SLC2A10* mutations, we conducted RNA-seq analysis on skin fibroblasts derived from ATS patients as described previously [25,35].

KEGG pathway analysis highlighted downregulation of ROS-regulated pathways such as the TNF signaling pathway, NF-kappa B signaling pathway, and NOD-like receptor signaling pathway, further supporting the role of altered ROS dynamics in ATS pathology [36,37].

RNA-seq in ATS skin fibroblasts indicates upregulation of *SFRP* and *DKK1*. Frizzled-related protein 1 (*SFRP1*), which is an antagonist of Wnt signaling, was identified as the most significantly upregulated gene, displaying a fold change of 7.31 in fibroblasts from ATS patients (Table 1). *SFRP1* is oversecreted upon cellular senescence caused by DNA damage or oxidative stress [38]. Wnt signaling inhibited by *SFRP1* increases the angiogenesis in mesenchymal cells, glioma cells and chorioallantoic membrane, making the blood vessels larger, longer and more mature and promoting the migration of endothelial cells (ECs) [39]. Additionally, SFRP1's interaction with Wnt receptors Fzd4 and Fzd7 aids in the cytoskeletal reorganization of ECs, thereby augmenting neovascularization during ischemia-induced angiogenesis in the hindlimbs of mice [39]. These mechanisms underscore the potential role of *SFRP1* in the vascular patterning defects in ATS and justify further research. Dickkopf-1 (*DKK1)* is a secreted Wnt/β-catenin pathway antagonist involved in embryogenesis. We found a 2.69-fold increase in fibroblasts from ATS patients (Table 1) [40]. Of note, enhanced expression of DKK1 in advanced carotid plaques suggests the potential operation of a DKK1-driven inflammatory loop within the atherosclerotic lesion [41].

KRT14 is downregulated in patient skin-derived fibroblasts. KRT14 is a direct interaction partner of Receptor-interacting protein kinase 4 (*RIPK4*) [42], a negative regulator of TGF-β signaling pathway in keratinocytes. Over-expression of *RIPK4* reduces TGF-β1-induced Smad2/Smad3 phosphorylation levels, whereas kinase dead *RIPK4* overexpression in HaCaT cells abolished its suppressive effect on Smad2/3 nuclear localization [43]. Hence, decreased *KRT14* levels may be related to TGF-β modulation in ATS through its direct RIPK4 interaction. Also, the interaction between β-catenin and *RIPK4* via the Dishevelled pathway suggests a potential synergistic effect with the upregulation of Wnt antagonists like *SFRP1*. Furthermore, we found a nearly 3-fold upregulation of Fibrillin-2 (*FBN2*) in fibroblasts from ATS patients suggest its crucial role in TGF-β signaling pathway in the pathology of elastic fiber disorganization and failed elastogenesis that resulting in connective tissue disorders [44]. Finally, Growth differentiation factor 10 *(GDF10)*, also known as Bone morphogenetic protein 3B (*BMP-3B*) is downregulated in ATS patients (Table 1). This divergent member of the TGF-β superfamily influences osteoblast differentiation and can inhibit this process similar to BMP3 [45]. *GDF10* has been identified as a negative regulator of vascular calcification [46]. Therefore, downregulation of *GDF10* in ATS may contribute to vascular calcification and reduced vascular elasticity through impaired regulation of osteogenic signaling pathways.

Paired-like homeodomain transcription factor 2 (*PITX2*) was found to be upregulated. *PITX2* regulates procollagen lysyl hydroxylase (*PLOD*) and *Dlx2* expression. *PLOD1* encodes an enzyme responsible for hydroxylating lysines in collagens that plays a role in specifying the ECM and provides a foundation for the morphogenesis of tissues and organs [47]. *Dlx2* encodes a transcription factor expressed in the mesenchymal and epithelial cells of the mandibular and maxillary regions, as well as in the diencephalon, and is established as a regulator of branchial arch development [48]. Moreover, the Wnt/Dvl/β-catenin→Pitx2 pathway regulates cell proliferation in specific tissues by modulating the expression of cell cycle genes like *Cyclin D2* through the induction of Pitx2 and subsequent coactivator recruitment [49]. *Pitx2* is expressed in the cardiac neural crest, guiding cell migration from the dorsal neural tube through the branchial arches. Defective proliferation in *Wnt-1 Cre/β-catenin*^{flox} and *Pitx2*$^{-/-}$ mice leads to reduced cell presence in the outflow tract and inadequate septation of the great arteries [50]. Therefore, upregulation of *PITX2* in ATS may contribute to abnormal extracellular matrix remodeling and vascular morphogenesis through its regulation of collagen-modifying enzymes and developmental pathways.

EPH receptor B2 (*EPHB2*), which acts downstream of Notch, is upregulated in ATS fibroblasts (Table 1) [51]. *EPHB2* has a role in platelet aggregation and activation, while also playing a key role in arterial endothelial cell growth during angiogenesis. Dysregulation of EphB2 signaling in ATS patients could therefore contribute to the characteristic arterial abnormalities and delayed wound healing observed.

Finally, altered expression of Collagen type IV alpha 4 chain (*COL4A4*), and Claudin *1* (*CLDN1*) may result in aberrant basal membrane patterning and tight junction formation indicating a role for cell-cell interactions and endothelial cell permeability.

Although the precise reason for the transcriptomic differences between Patient 1 and Patient 2 remains unclear, they are most likely attributable to technical variability or individual-specific biological factors. KEGG pathway and Gene On-

tology (GO) annotation analyses of RNA-seq data from both patients revealed distinct regulatory alterations in biological processes that may contribute to the pathophysiology of ATS. Notably, both patients demonstrated significant down-regulation of cardiovascular and immune-related pathways, potentially contributing to the structural and functional abnormalities observed in the arterial system. As shown in Table 2, pathways essential for cardiovascular function—such as hypertrophic cardiomyopathy (HCM) and arrhythmogenic right ventricular cardiomyopathy (ARVC)—were down-regulated in both cases, supporting a molecular basis for the increased arterial tortuosity phenotype.

In contrast, the opposite directionality observed in the cell adhesion molecules (CAMs) pathway may reflect patient-specific variation in cellular adhesion dynamics and extracellular matrix remodeling. This divergence may be associated with differences in genetic background, disease severity, or compensatory responses to GLUT10 deficiency, and may indicate heterogeneity in the molecular response to ATS.

In Patient 1, GO annotation highlighted significant down-regulation of pathways related to immune response, angiogenesis, and structural maintenance, and up-regulation of cell adhesion, mitotic nuclear division, and G1/S transition (Table 3). In contrast, Patient 2 exhibited down-regulation in structural and cell adhesion-related pathways, accompanied by up-regulation of pathways promoting cell proliferation and migration.

This study provides preliminary insights into transcriptomic alterations in fibroblasts from ATS patients; however, several limitations should be considered. The small sample size limits the generalizability of the findings, and larger cohorts are required to validate the identified DEGs. Although dysregulated pathways were identified, functional validation of key genes such as *SFRP1*, *DKK1*, and *FBN2* is necessary to clarify their roles in ECM remodeling. In addition, the mechanisms linking GLUT10 deficiency, elevated ROS, and non-canonical TGF-β signaling remain to be elucidated. Future studies, including in vitro and in vivo models as well as analyses in additional cell types such as vascular smooth muscle and endothelial cells, are needed to better understand ATS pathophysiology.

5. Conclusions

Our RNA-seq analysis of fibroblasts derived from two ATS patients provides preliminary insights into the molecular effects of *SLC2A10* mutations. The results suggest alterations in extracellular matrix organization, vascular integrity, and multiple signaling pathways, including Wnt, TNF, and NF-kappa B pathways. These findings contribute to a better understanding of ATS pathogenesis and highlight dysregulated pathways that may be relevant to disease mechanisms.

Conflict of interest

The authors declare that they have no competing interests.

Acknowledgements

We heartfully thank the families for their participation and valuable support to this study.

Ethical Review and Approval

The research was conducted ethically in accordance with the World Medical Association Declaration of Helsinki and local institutional ethics committee rules. Ethical approval was obtained from the Bursa Uludag University Health Research Ethics Committee (Decision No: 2026/189/6-36)

References

1. Coucke PJ, Willaert A, Wessels MW, Callewaert B, Zoppi N, De Backer J, Fox JE, Mancini GM, Kambouris M, Gardella R, Facchetti F, Willems PJ, Forsyth R, Dietz HC, Barlati S, Colombi M, Loeys B, De Paepe A. Mutations in the facilitative glucose transporter GLUT10 alter angiogenesis and cause arterial tortuosity syndrome, Nat Genet. 2006;38(4):452–457.
2. Ertugrul A. Diffuse tortuosity and lengthening of the arteries. Circulation. 1967;36(3):400-407.
3. Pletcher BA, Fox JE, Boxer RA, Singh S, Blumenthal D, Cohen T, Brunson S, Tafreshi P, & Kahn E. Four sibs with arterial tortuosity: Description and review of the literature. Am J Med Genet. 1996;66(2):121–128.
4. Wessels MW, Catsman-Berrevoets CE, Mancini GM, Breuning MH, Hoogeboom JJ, Stroink H, Frohn-Mulder I, Coucke PJ, Paepe AD, Niermeijer MF, & Willems PJ. Three new families with arterial tortuosity syndrome. Am J Med Genet. 2004;*131*(2):134–43.
5. Hardin JS, Zarate YA, Callewaert B, Phillips PH, Warner DB. Ophthalmic findings in patients with arterial tortuosity syndrome and carriers: A case series. Ophthalmic Genet. 2018;39(1):29–34.
6. Hasler S, Stürmer J, Kaufmann C. Keratoglobus and deep stromal corneal opacification in a case of arterial tortuosity syndrome. Klin Monbl Augenheilkd. 2011;228(4):345–346.
7. Beyens A, Albuisson J, Boel A, Al-Essa M, Al-Manea W, Bonnet D, Bostan O, Boute O, et al. Arterial tortuosity syndrome: 40 new families and literature review. Genetics in Medicine. 2018;20(10):1236–45.
8. Albuisson J, Moceri P, Flori E, Belli E, Gronier C, Jeunemaitre X. Clinical utility gene card for: Arterial tortuosity syndrome. European Journal of Human Genetics. 2015;23:8–10.
9. Callewaert BL, Willaert A, Kerstjens-Frederikse WS, De Backer J, Devriendt K. et al. Arterial Tortuosity Syndrome: Clinical and Molecular Findings in 12 Newly Identified Families. Hum Mutation. 2008;29(1):150–8.
10. Joost Hans-Georg TB. The extended GLUT-family of sugar/polyol transport facilitators: nomenclature, sequence characteristics, and potential function of its novel mem-

bers. Mol Membr Biol. 2001;18(4):247–256.
11. Long W, Cheeseman CI. Structure of, and functional insight into the GLUT family of membrane transporters. Cell Health Cytoskelet. 2015;7:167–183.
12. Dawson PA, Mychaleckyj JC, Fossey SC, Mihic SJ, Craddock AL, Bowden DW. Sequence and Functional Analysis of GLUT10: A glucose transporter in the type 2 diabetes-linked region of chromosome 20q12-13.1. Mol Genet Metab. 2001;74:186–99.
13. McVie-Wylie AJ, Lamson DR, Chen YT. Molecular cloning of a novel member of the GLUT family of transporters, SLC2A10 (GLUT10), localized on chromosome 20q13.1: A candidate gene for NIDDM susceptibility. Genomics. 2001;72(1):113–7.
14. Segade F. Glucose transporter 10 and arterial tortuosity syndrome: The vitamin C connection. FEBS Lett. 2010;584:2990–4.
15. Lee YC, Huang HY, Chang CJ, Cheng CH, Chen YT. Mitochondrial GLUT10 facilitates dehydroascorbic acid import and protects cells against oxidative stress: Mechanistic insight into arterial tortuosity syndrome. Hum Mol Genet. 2010;19:3721–33.
16. Gamberucci, A, Marcolongo, P, Németh CE, Zoppi N., Szarka, A, et al. GLUT10—lacking in arterial tortuosity syndrome—is localized to the endoplasmic reticulum of human fibroblasts. Int J Mol Sci. 2017;18(8):1820.
17. Zoppi N, Chiarelli N, Cinquina V, Ritelli M, Colombi M. GLUT10 deficiency leads to oxidative stress and non-canonical αvβ3 integrin-mediated TGFβ signalling associated with extracellular matrix disarray in arterial tortuosity syndrome skin fibroblasts. Hum Mol Genet. 2015;24:6769–87.
18. Loeys BL, Chen J, Neptune ER, Judge DP, Podowski M, et al. A syndrome of altered cardiovascular, craniofacial, neurocognitive and skeletal development caused by mutations in TGFBR1 or TGFBR2. Nature Genetics. 2005;37(3):275–281.
19. Wight TN, Merrilees MJ. Proteoglycans in atherosclerosis and restenosis: Key roles for versican. Circ Res. 2004;94(9):1158–67.
20. Gardella R, Zoppi N, Assanelli D, Muiesan ML, Barlati S, Colombil M. Exclusion of Candidate Genes in a Family with Arterial Tortuosity Syndrome. Am J Med Genet. 2004;126A(3):221–8.
21. Boel, A., Veszelyi, K., Németh, C. E., Beyens, A., Willaert, A., Coucke, P., Callewaert, B., & Margittai, É. Arterial Tortuosity Syndrome: An Ascorbate Compartmentalization Disorder? Antioxid Redox Signal.2021;34(11):875–89.
22. Willaert A, Khatri S, Callewaert BL, Coucke PJ, Crosby SD, Lee JG, Davis EC, Shiva S, Tsang M, De Paepe A, Urban Z. GLUT10 is required for the development of the cardiovascular system and the notochord and connects mitochondrial function to TGFβ signaling. Hum Mol Genet. 2011;21(6):1248–59.
23. Callewaert BL, Loeys BL, Casteleyn C, Willaert A, Dewint P, De Backer J, Sedlmeier R, Simoens P, De Paepe AM, & Coucke PJ. Absence of arterial phenotype in mice with homozygous slc2A10 Missense substitutions. Genesis. 2008;46:385–9.
24. Boel, A., Burger, J., Vanhomwegen, M., Beyens, A., Renard, M., Barnhoorn, S., Casteleyn, C., Reinhardt, D. P., Descamps, B., Vanhove, C., van der Pluijm, I., Coucke, P., Willaert, A., Essers, J., & Callewaert, B. Slc2a10 knockout mice deficient in ascorbic acid synthesis recapitulate aspects of arterial tortuosity syndrome and display mitochondrial respiration defects. Hum Mol Genet. 2020;29(9):1476–1488.
25. Richards, S., Aziz, N., Bale, S., Bick, D., Das, S., Gasti-er-Foster, J., Grody, W. W., Hegde, M., Lyon, E., Spector, E., Voelkerding, K., Rehm, H. L., & ACMG Laboratory Quality Assurance Committee. Standards and guidelines for the interpretation of sequence variants: A joint consen-sus recommendation of the American College of Medical Genetics and Genomics and the Association for Molecular Pathology. Genetics in Medicine. 2015;17(5):405–424.
26. Kim, A. H., Sakin, I., Viviano, S., Tuncel, G., Aguilera, S. M., Goles, G., Jeffries, L., Ji, W., Lakhani, S. A., Kose, C. C., Silan, F., Oner, S. S., Kaplan, O. I., MarmaRare Group, Ergoren, M. C., Mishra-Gorur, K., Gunel, M., Sag, S. O., Temel, S. G., & Deniz, E. CC2D1A causes ciliopathy, in-tellectual disability, heterotaxy, renal dysplasia, and abnor-mal CSF flow. Life Sci Alliance. 2024;7:e202402708.
27. Vangipuram, M., Ting, D., Kim, S., Diaz, R., & Schüle, B.(2013). Skin punch biopsy explant culture for derivation of primary human fibroblasts. Journal of visualized experi-ments: JoVE, 77, e3779.
28. Emisoglu-Kulahli H, Gul S, Morgil H, Ozcan O, Aygenli F, Selvi S, Kavakli IH, Ozturk N. Transcriptome analysis of the circadian clock gene BMAL1 deletion with opposite carcinogenic effects. Funct Integr Genomics. 2021;21(1):1–16.
29. Sarayloo E, Tardu M, Unlu YS, Simsek S, Cevahir G, Erkey C, et al. Understanding lipid metabolism in high-lipid-producing Chlorella vulgaris mutants at the genome-wide level. Algal Res. 2017;28:244–52.
30. Cavga AD, Tardu M, Korkmaz T, et al. Cryptochrome deletion in p53 mutant mice enhances apoptotic and anti-tumorigenic responses to UV damage at the transcriptome level. Funct Integr Genomics.2019;19:729–42.
31. Bolger AM, Lohse M, Usadel B. Trimmomatic: A flexible trimmer for Illumina sequence data. Bioinformatics. 2014;30(15):2114–20.
32. Dobin A, Davis CA, Schlesinger F, Drenkow J, Zaleski C, Jha S, et al. STAR: Ultrafast universal RNA-seq aligner. Bioinformatics. 2013;29(1):15–21.
33. Trapnell C, Roberts A, Goff L, et al. Differential gene and transcript expression analysis of RNA-seq experiments with TopHat and Cufflinks. Nat Protoc. 2012;7(3):562–78.
34. Bindea G, Mlecnik B, Hackl H, et al. ClueGO: A Cytoscape plug-in to decipher functionally grouped gene on-

tology and pathway annotation networks. *Bioinformatics*. 2009;25(8):1091–1093.
35. Németh, CE, Nemoda Z, Lőw P, Szabó P, Horváth EZ, Willaert A, Boel A, Callewaert BL, Coucke PJ, Colombi M, Bánhegyi G, & Margittai É. Decreased nuclear ascorbate accumulation accompanied with altered genomic methylation pattern in fibroblasts from arterial tortuosity syndrome patients. Oxid Med Cell Longev. 2019;8156592.
36. Morgan MJ, Liu ZG. Crosstalk of reactive oxygen species and NF-κB signaling. Cell Res. 2011;21(1):103–15.
37. Morgan MJ, Liu ZG. Reactive oxygen species in TNFα-induced signaling and cell death. Mol Cells. 2010;30(1):1–12.
38. Elzi DJ, Song M, Hakala K, Weintraub ST, Shiio Y. Wnt Antagonist SFRP1 Functions as a Secreted Mediator of Senescence. Mol Cell Biol. 2012;32(21):4388–99.
39. Dufourcq P, Leroux L, Ezan J, et al. Regulation of endothelial cell cytoskeletal reorganization by a secreted frizzled-related protein-1 and frizzled 4-and frizzled 7-dependent pathway: Role in neovessel formation. *American Journal of Pathology*. 2008;172(1):37–49.
40. Logan CY, Nusse R. The Wnt signaling pathway in development and disease. Annu Rev Cell Dev Biol. 2004;20:781–810.
41. Ueland T, Otterdal K, Lekva T, Halvorsen B, Gabrielsen A, Sandberg WJ, Paulsson-Berne G., Pedersen TM. et al. Dickkopf-1 enhances inflammatory interaction between platelets and endothelial cells and shows increased expression in atherosclerosis. Arterioscler Thromb Vasc Biol. 2009;29(8):1228–34.
42. Sümer C, Boz Er AB, Dinçer T. Keratin 14 is a novel interaction partner of keratinocyte differentiation regulator:receptor-interacting protein kinase 4. Turkish Journal of Biology. 2019;43(4):225–34.
43. Dinçer T, Boz Er AB, Er İ, Toraman B, Yildiz G, Kalay E. RIPK4 suppresses the TGF-β1 signaling pathway in HaCaT cells. Cell Biol Int. 2020;44(3):848–60.
44. Van Loon K, Yemelyanenko-Lyalenko J, Margadant C, Griffioen AW, Huijbers EJM. Role of fibrillin-2 in the control of TGF-β activation in tumor angiogenesis and connective tissue disorders. Biochim Biophys Acta Rev Cancer. 2020;1873(2):188354.
45. Cunningham NS, Jenkins NA, Gilbert DJ, Copeland NG, Reddi AH, Lee SJ. Growth/differentiation factor-10: A new member of the transforming growth factor-β superfamily related to bone morphogenetic protein-3. Growth Factors. 1995;12(2):99–109.
46. Platko K, Gyulay G, Lebeau PF, MacDonald ME, Lynn EG, Byun JH, Igdoura SA, Holden, RM, et al. GDF10 is a negative regulator of vascular calcification. Journal of Biological Chemistry. 2024;300(11):1–14.
47. Hjalt TA, Amendt BA, Murray JC. PITX2 regulates procollagen lysyl hydroxylase (PLOD) gene expression: Implications for the pathology of Rieger syndrome. Journal of Cell Biology. 2001;152(3):545–52.
48. Qiu M, Juanito J. Null mutation of Dlx-2 results in abnormal morphogenesis of proximal first and second branchial arch derivatives and abnormal differentiation in the forebrain. Genes Dev. 1995;9(20):2523–38.
49. Kioussi C, Briata P, Baek SH, Rose DW, Hamlet NS, Herman T, Ohgi K, Lin C, et al. Identification of a Wnt/Dvl/β-Catenin → Pitx2 Pathway Mediating Cell-Type-Specific Proliferation during Development cell-type-specific proliferation during development. Cell. 2002;111(5):673–85.
50. Grego-Bessa J, Luna-Zurita L, del Monte G, Bolós V, Melgar P, Arandilla A, et al. Notch Signaling Is Essential for Ventricular Chamber Development. Dev Cell. 2007;12(3):415–29.
51. Vaiyapuri S, Sage T, Rana RH, Schenk MP, Ali MS, Unsworth AJ, Jones CI, Stainer AR et al. EphB2 regulates contact-dependent and contact-independent signaling to control platelet function. Blood. 2015;125(4):720–31.